Simultaneous surface pressure and high-speed PIV measurements in stalled airfoil

Tim Berk[1], Giovanni Lacagnina[2], Paruchuri Chaitanya[2], Phillip Joseph[2], Bharathram Ganapathisubramani[1,*]
1: Aerodynamics and Flight Mechanics Research Group, University of Southampton, Southampton, UK
2: Institute of Sound and Vibration Research, University of Southampton, Southampton, UK
* Correspondent author: G.Bharath@southampton.ac.uk

ABSTRACT

The time-resolved velocity field (2D2C high-speed PIV) and surface pressure (pressure taps) of a stalled NACA0012 airfoil have been simultaneously measured. These measurements enable cross-evaluation of the velocity field and pressure time series. The present paper evaluates the flow field and surface pressure using POD, cross-correlation and conditional averaging. First, the flow and surface pressure are analysed independently. Both the time-average and the dynamic structures of the flow are presented. Distinct frequency bands are observed in the energy spectra of the surface-pressure signal. It is shown that a high-pressure event at the foremost pressure port (at x/c = 0.34) is followed by high-pressure events at the other pressure ports (x/c = 0.51–0.93), indicating a decaying pressure wave that travels over the surface with roughly half the free-stream velocity. Next, the link between the flow field and the surface pressure is explored. Using cross-correlation, it is shown that the pressure signal correlates with specific regions in the flow. Conditional averages of the flow fields, conditioned to high-pressure events at the surface, indicate that these pressure events are caused by coherent structures in the flow. These structures consist of a train of alternating vortices that induce velocity components toward and away from the surface, causing high- and low-pressure events at this surface. By filtering the pressure signal with different frequency bands, the flow structures responsible for different peaks in the energy spectra are recovered. A POD analysis indicates that the energy of the coherent flow structures leading to surface-pressure fluctuations only contain a fraction of the total energy of the flow. While POD and cross-correlation are applied to a full time-series, the conditional averages show that coherent structures in the flow can be identified in real-time using the surface pressure. Identification of coherent structures in the flow using only the surface pressure signal enables real-time control of such structures.

1. Introduction

The separated flow over the suction side of an airfoil is a dynamic region filled with vortical structures (e.g. Burgmann *et al.* (2006)). The vortical structures in a separated flow have been shown to correlate with surface-pressure fluctuations (e.g. Kiya and Sasaki (1985), Iaccarino *et al.* (2003)). The dominant modes (containing most energy) can be identified using a model reduction method such as POD (Proper Orthogonal Decomposition) or DMD (Dynamic Mode Decomposition) (Thomareis and Papadakis, 2017). DMD has been used to identify structures in the flow over both static airfoils (Thomareis and Papadakis, 2017) and dynamic airfoils (Mariappan *et al.*, 2014, Dunne and McKeon, 2015). Identification of structures in the flow can be

used for flow control purposes such as separation control. In (active) separation control, the flow is forced with the goal of delaying flow separation (e.g. Amitay and Glezer (2002)). Identification of structures in the flow can help actively targeting these structures. To target these structures, they need to be identified in real-time, which makes model reduction methods such as POD and DMD (which are applied to a full time-series) inapplicable. The present study investigates the correlation between structures in the flow and the surface pressure on the airfoil. The goal is to explore the use of the surface-pressure signal to identify structures in the flow.

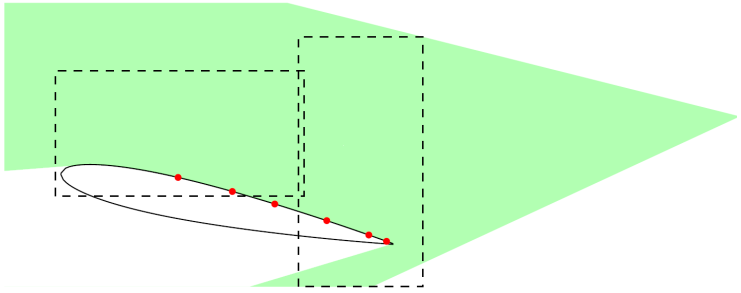

Fig. 1 Schematic of set-up showing the PIV fields-of-view (dashed lines) and surface-pressure ports (red dots).

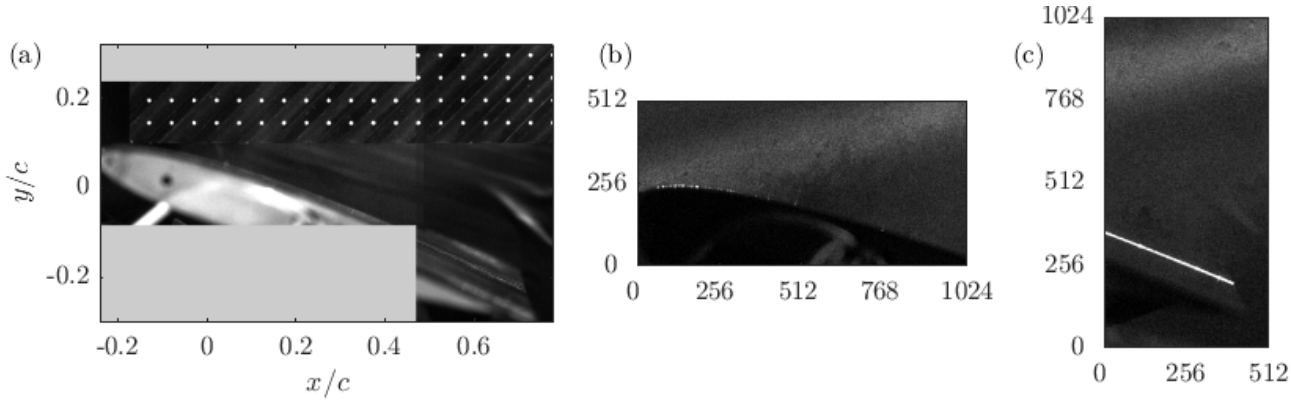

Fig. 2 Stitched calibration images (a) and examples of raw data (b, LE) and (c, TE).

2. Experimental set-up

A two-dimensional NACA0012 airfoil section with chord length c = 0.2 m is placed at a geometric angle-of-attack of α' = 17 degrees in an open-jet wind tunnel at a free-stream velocity of U_∞ = 20 m/s. The combination of the airfoil chord and nozzle size of the open jet with the geometric angle-of-attack leads to an effective angle-of-attack of $\alpha \approx 10$ degrees (see Brooks et al. (1984)). The flow over the airfoil is fully separated (stalled). The airfoil section is installed in the open jet wind tunnel facility of the Institute of Sound and Vibration Research at the University of Southampton. This facility is housed in an anechoic chamber of 8 m by 8 m by 8 m which enables accurate far-field noise measurements for future studies. See Figure 1 for a schematic of the set-up.

The velocity field over the airfoil is measured using highspeed-PIV. The flow is seeded using a Magnum Martín smoke machine which generates smoke particles with a diameter of 1 μm. Particles are illuminated using a dual-pulse Nd:YLF laser (Litron Lasers LDY 304), creating an approximately 1 mm thick laser sheet at mid-span on the suction side of the airfoil. Images are recorded using two highspeed cameras (Phantom v641) operated with a resolution of 1024 by 512 pixels (0.5 MP), positioned in a T-shape as shown in Figures 1 and 2a. Examples of raw images of both cameras are shown in Figures 2b and c. Image pairs are recorded with a time separation of dt = 50 μs at a recording rate of 4 kHz. The 32 GB memory cameras can record 21393 image pairs, leading to samples of just over T = 5.3 s (or $T\,U_\infty/c$ = 530 turn-over times of the flow over the airfoil). Three runs are recorded, giving 802 turn-over times in total. Images are recorded and processed using LaVision DaVis. Images are pre-processed by removing the (temporal) minimum of the entire dataset, followed by removing a (spatial) sliding minimum. Vectors are determined using GPU multi-pass processing with a final step of square windows measuring 32 by 32 pixels (75% overlap), leading to a resolution of 1.1 mm per vector.

The airfoil is fitted with pressure taps located at the spanwise centre (aligned with the laser sheet) at x/c = 0.34, 0.505, 0.635, 0.795, 0.925 and 0.98. These pressure taps are connected to 2.5 mm diameter omnidirectional electret condenser microphones (Knowles Electronics FG-3329-P07). These microphones are connected to a T-junction with a 3 m long tube leading away from the third leg of the junction in order to avoid reflections. The microphones are calibrated individually in-situ against a reference B&K 0.5 inch condenser microphone. Velocity fields and surface pressure are acquired simultaneously and camera-trigger signals are used for synchronisation.

3. Results and discussion

In this section the flow-field and pressure signal are first analysed independently. Next, they are evaluated together by analysing cross-correlation maps of the flow and the surface pressure and by taking conditional averages of the velocity fields conditioned to high-pressure events at the surface.

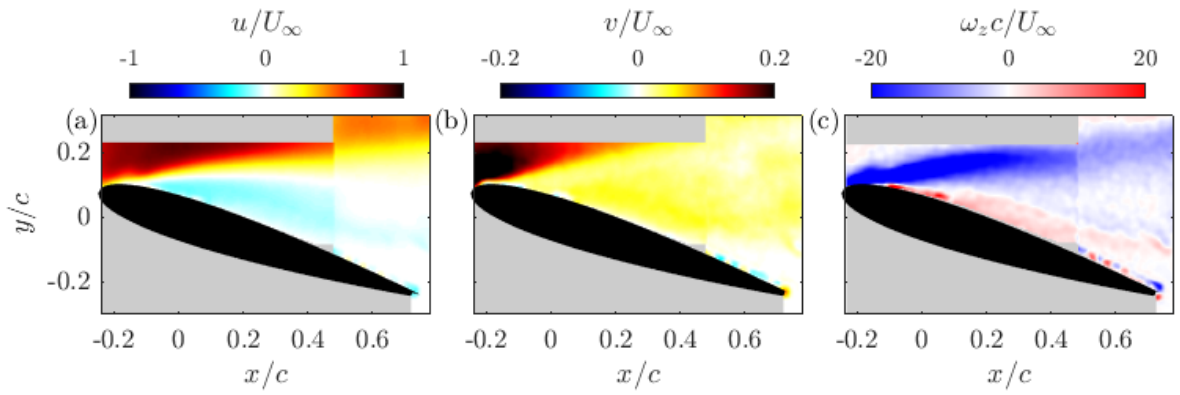

Fig. 3 Time-averaged flow fields showing horizontal velocity component (a), vertical velocity component (b) and spanwise vorticity component (c).

3.1. Time-averaged flow

The time-averaged velocity and vorticity fields are presented in Figure 3. The horizontal velocity component (a) indicates a time-averaged separation close to the leading edge. Behind the separated shear layer a significant flow reversal is observed in the recirculation region. This leads to a positive (upward) vertical velocity in almost the entire field-of-view as presented in (b). The spanwise-vorticity field (c) indicates a strong shear layer caused by the separation (negative vorticity, blue). The boundary layer of the reversing flow on top of the airfoil can also be observed (positive vorticity, red).

3.2. Dynamic structure of the flow (POD)

Due to turbulent fluctuations, coherent structures in the flow (such as a moving separated shear layer or shed vortices) are hard to observe in instantaneous images. Proper orthogonal decomposition (POD) groups coherent energetic structures (modes) of a data set (see for example Sirovich (1987)). POD modes of the current data-set are determined based on a subset of 4000 images, using only the upstream camera. The six most energetic modes are presented in Figure 4. Each subfigure shows the normalized magnitude of velocity fluctuations $(u'_{POD}{}^2 + v'_{POD}{}^2)^{0.5}$ in the given mode. The relative contribution of the energy in each mode (E) is indicated in each subfigure. Even the most energetic dynamic modes contain only about 1% of the total energy of the velocity fluctuations in the flow and about 200 of the 4000 modes are required to represent 50% of the energy of the flow. This suggests that the flow is dominated by random fluctuations rather than coherent structures.

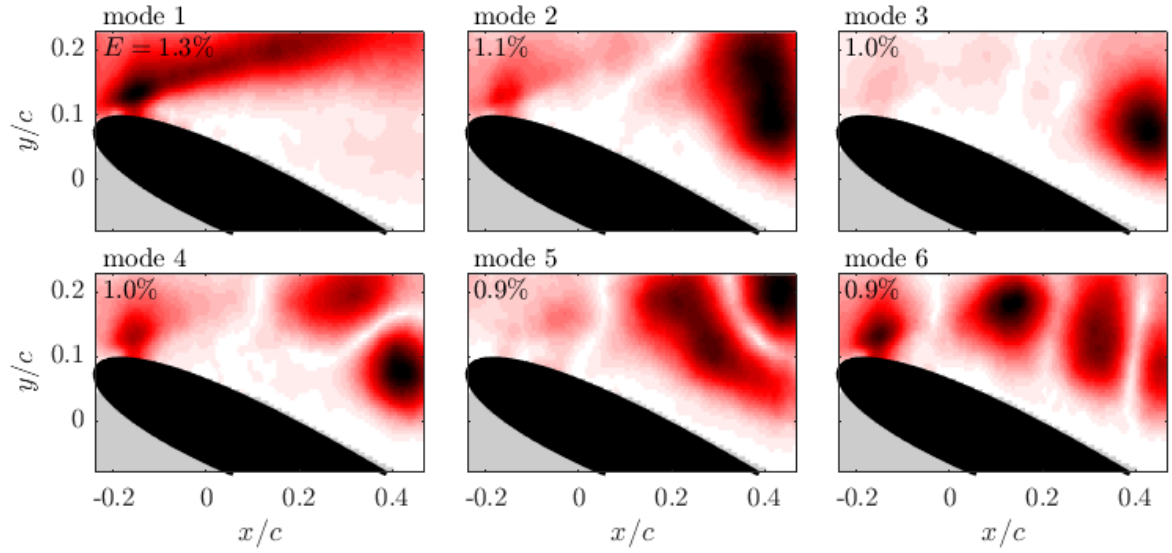

Fig. 4 Six most energetic POD mode shapes of velocity fluctuations $(u'_{POD}{}^2 + v'_{POD}{}^2)^{0.5}$. Relative energy of each mode (%) is indicated in each figure.

3.3. Surface pressure fluctuations

The pre-multiplied power spectral density of the foremost pressure tap (x/c = 0.34) is presented in Figure 5a. Two main peaks can be identified at 25 and 100 Hz, indicated by the dashed lines. Using cut-off frequencies at 50 and 200 Hz leads to three frequency bands, where the first band (f < 50 Hz) is associated with the first peak, the second band (f = 50–200 Hz) is associated with the second peak and the third band (f > 200 Hz) with the higher frequencies. These frequency bands are isolated using Butterworth low-pass, band-pass and high-pass filters respectively. A sample of the pressure signal time-series is presented in Figure 5b. The full signal (black line) is overlaid with the low-pass filtered (blue), the band-pass filtered (red) and the high-pass filtered signal (green). The magnitude of each signal is normalized by their respective standard deviation ($\sigma(p)$), causing the amplitudes to be similar. The black dashed lines ($\pm\,\sigma$) indicate limits for identifying low- and high-pressure events. A normalized histogram of the band-passed signal (red-coloured line in (b)) is presented in (c). This histogram shows a seemingly Gaussian distribution. All events that are identified as high- or low-pressure events are dark-coloured. Both these groups comprise of approximately 15% of the signal.

The signal of all pressure ports can be evaluated conditioned to the signal of the foremost pressure port. The signal at each port is averaged over times $t = (t_0 + \Delta t)$ for which the foremost port had a high pressure signal at $t = t_0$, i.e.

$$p_i(\Delta t) = \langle p_i(t_0 + \Delta t)|_{p_1(t_0)>\sigma(p)}\rangle, \qquad (1)$$

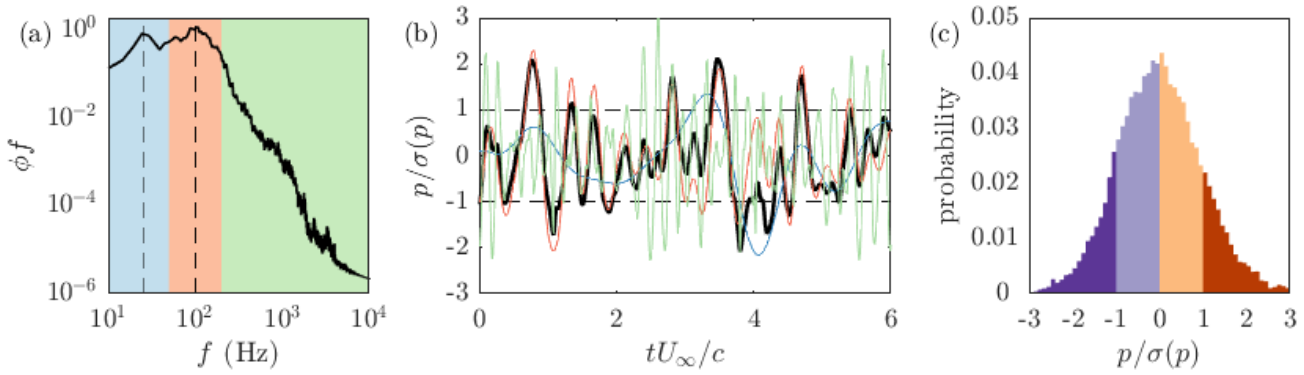

Fig. 5 Surface pressure measured at foremost pressure tap. Pre-multiplied energy spectra (a). Pressure signal (b) of the unfiltered signal (black), f < 50 Hz low-pass filtered (blue), f = 50-200 Hz band-pass filtered (red) and f > 200 Hz high-pass filtered (green). Dashed lines indicate limits for identification of low- and high-pressure events. Normalized histogram of the band-pass filtered signal, indicating the relative number of low- and high-pressure events.

where $\langle X \rangle$ denotes a time-average of X and $X|_{p>\sigma(p)}$ denotes conditioning of X to times for which $p>\sigma(p)$. The pressure signal of the six different ports – conditioned to high pressure at the foremost port – as function of the time-lag is presented in Figure 6a (colours correspond to pressure-port locations in (b) and (c)). The time evolution indicates a pressure wave that appears at the foremost port first and travels towards the trailing edge while decreasing in magnitude. The time-lag of each peak as function of the location on the airfoil is presented in (b). The evolution velocity is relatively constant and approximately half of the free-stream velocity. The decay of the peak with chordwise distance is presented in (c).

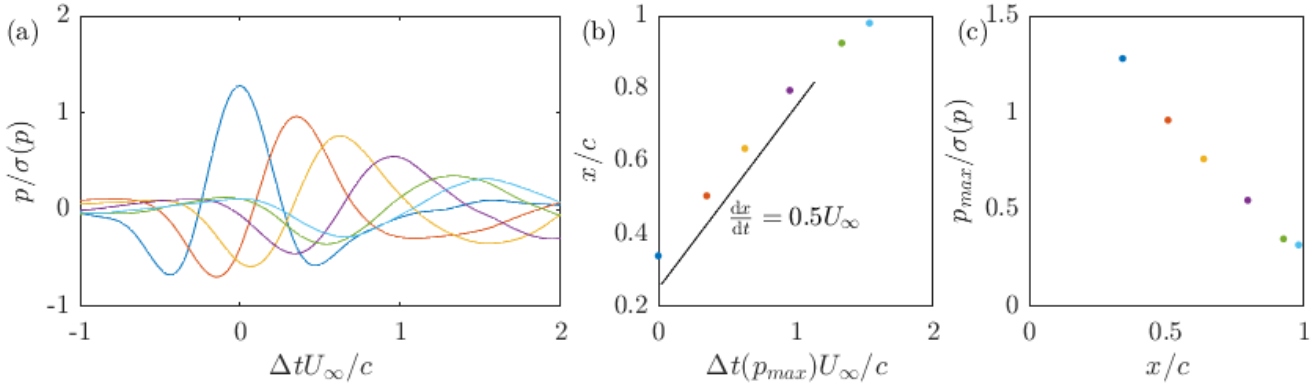

Fig. 6 Surface pressure at multiple ports, conditioned to high-pressure events at foremost pressure port. Pressure as function of time-lag (a) with the high-pressure event at the foremost port at Δt = 0. Time-evolution of the peak over the airfoil (b), indicating the propagation velocity of the pressure event. Decay of the peak (c).

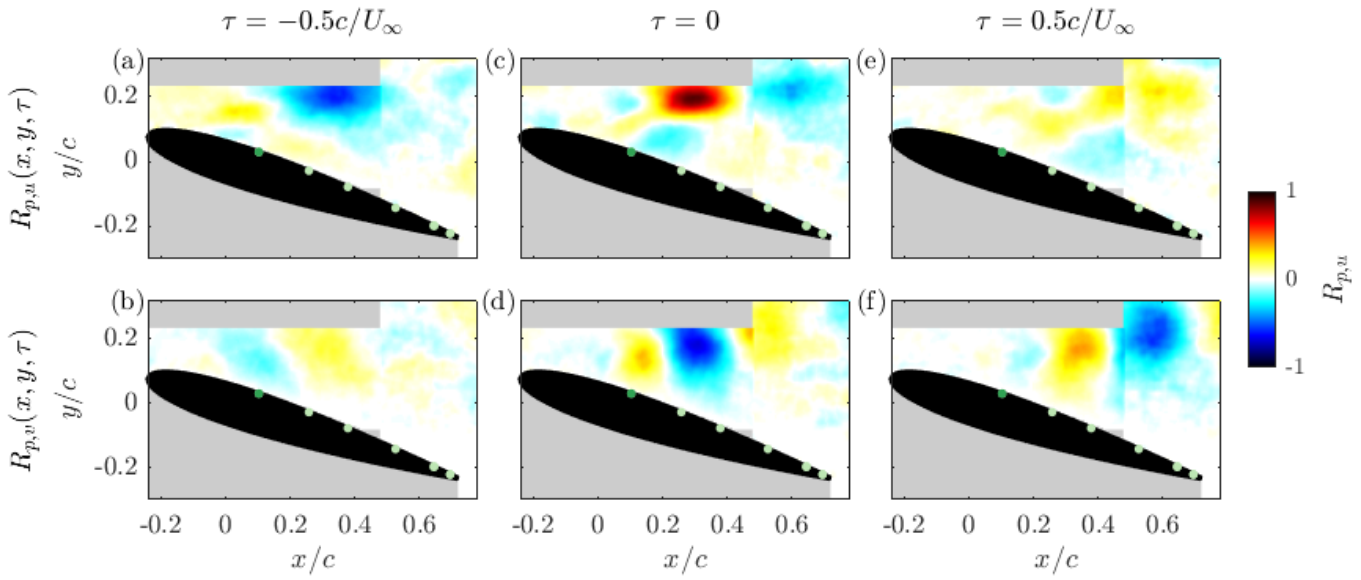

Fig. 7 Maps of the cross-correlation between the first pressure port and the horizontal (a, c, e) and vertical (b, d, f) velocity components. Correlations are evaluated at time-lags of τ = -0.5 c/U_∞ (a, b), τ = 0 (c, d) and τ = 0.5 c/U_∞ (e, f).

The advection of these pressure waves with half the free-stream velocity suggests that the pressure is a footprint of coherent structures in the shear layer (where the local velocity is lower than the free-stream velocity). In the following sections the link between the pressure and the flow is evaluated using multiple tools.

3.4. Correlation between surface pressure and flow

The similarity of the pressure signal with the velocity field is evaluated using cross-correlation. The cross-correlation of the surface pressure signal of a given pressure port with the flow is defined as

$$R_{p,u}(x,y,\tau) = \frac{1}{N}\sum_{n=1}^{N} p(n)u(x,y,n+\tau), \quad (2)$$

where n = 1–N are the indices of the discrete time signal and τ is the time-lag at which the correlation is evaluated. Cross-correlation maps of both components of velocity with the signal of the foremost pressure port are presented in Figure 7. The cross-correlation with zero time-lag is presented in 7c (u-component of velocity) and d (v-component). Both show alternating regions of high-positive and high-negative correlations between the velocity and surface pressure. The streamwise extent of these regions is roughly x/c = 0.25. The correlation maps with a time-lag corresponding to approximately the size of these regions (τ = ± 0.5 c/U_∞, using the obtained advection velocity of 0.5 U_∞) is presented in Figures 7a, b, e and f. These show that indeed these regions of high-positive and high-negative correlation have shifted (and decreased in magnitude). This suggests that these correlations are formed by coherent structures moving in the flow. High-

positive correlations are likely a result of velocities being high when surface pressure is high (and vice versa) while high-negative correlations are likely a result of velocities being high when surface pressure is low (and vice versa).

The next sections evaluate the flow field conditioned to high- and low-pressure events.

3.5. Conditionally averaged flow structures

Velocity fields are evaluated conditioned to the pressure at the foremost surface pressure port. An illustration of this conditioning is presented in Figure 8. In the left panel a small time-series of the band-pass filtered surface pressure is presented. High-pressure events are identified as parts of this time-series where $p(t)>\sigma(p)$. Snapshots of the velocity field during these events are presented in the middle panel. The snapshots during all high-pressure events are averaged as presented in the right panel. An important feature of this analysis is that velocity fields are not (spatially) filtered but are selectively chosen based on the surface pressure signal. While coherent structures in individual snapshots (middle panel of Fig. 8) might be overshadowed by turbulent fluctuations, these coherent structures become more apparent when averaging over multiple instances (right panel of Fig. 8).

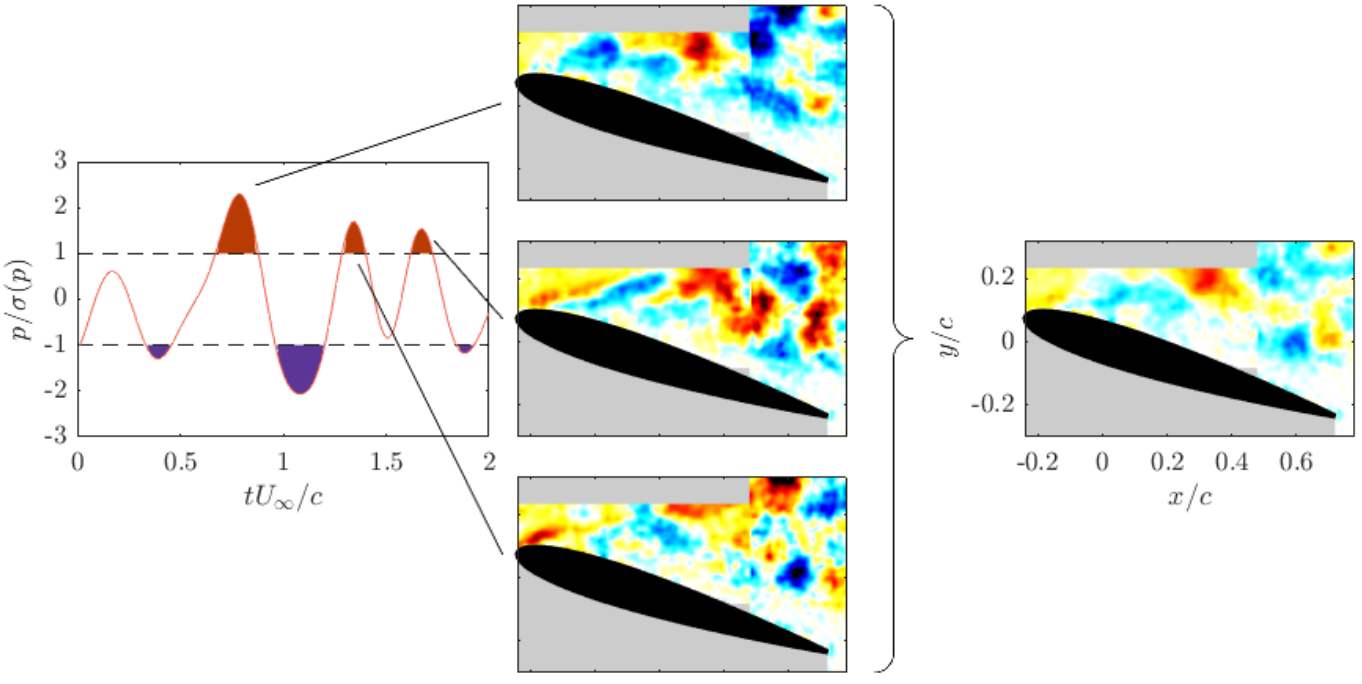

Fig. 8 Illustration of conditionally averaging method. Perturbed-streamwise-velocity (u') fields (middle panel) are selectively chosen based on high-pressure events (left) and time-averaged (right)

Velocity fields are presented with the unconditioned time-averaged signal subtracted, i.e.

$$u'(x,y) = \langle u(x,y,t)|_{p>\sigma(p)}\rangle - \langle u(x,y,t)\rangle \qquad (3)$$

The spanwise-vorticity is calculated using these velocity fields, i.e. $\omega_z' = \partial v'/\partial x - \partial u'/\partial y$. Velocity and vorticity fields conditioned to high- and low-pressure events in the raw pressure signal are presented in Figure 9. These flow fields indicate velocity perturbations as caused by a train of alternating vortices in the shear layer of the separated flow. These vortices induce alternating positive and negative velocity fluctuations. It is observed that the flow structures conditioned to high-pressure events are of opposite sign to the flow structures conditioned to low-pressure events. The downstream evolution of the train of vortices causes this alternating behaviour of positive and negative vortices, leading to velocity fluctuations alternating towards and away from the surface, which in turn leads to alternating high- and low-pressure events at the surface. The conditionally averaged velocity fields show great similarity to the cross-correlation maps (compare Fig. 9 a and b to Fig. 7 c and d), suggesting a linear relation between the velocity and surface pressure.

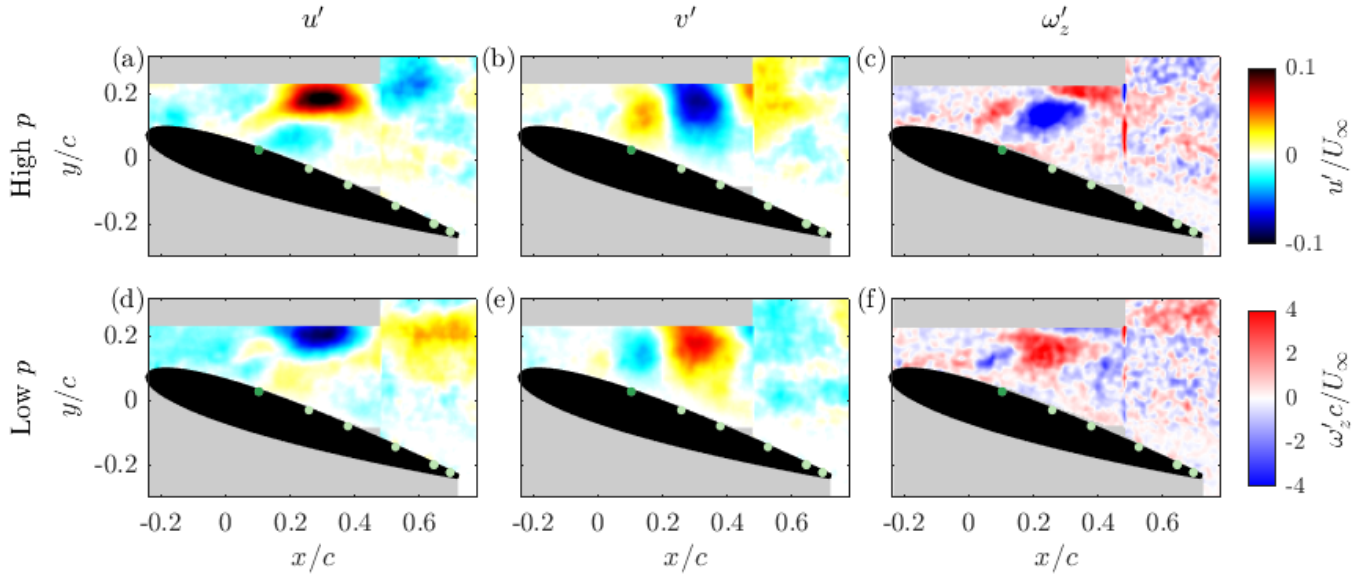

Fig. 9 Velocity and vorticity fields conditioned to high- (a, b and c) and low- (d, e and f) surface pressure events.

As discussed in Section 3.3 the surface-pressure signal can be divided into multiple frequency bands. The conditional averaging as used above can be applied to the filtered pressure signals to identify the dominant flow structures responsible for the different peaks in the surface-pressure energy spectrum.

The flow fields corresponding to low- and high-pressure events of the low-pass filtered ($f < 50$ Hz) surface pressure signal are presented in Figure 10. The frequency of the pressure signal can be written as a spatial wavelength using the propagation velocity of the pressure waves (0.5 U_∞) as advection velocity (applying Taylor's hypothesis), i.e. $\lambda_x = 0.5\ U_\infty/f$. It should be noted that these waves consist of a positive and negative part, meaning that the length of single flow structures is half of this wavelength, i.e. $l_x/c = 0.25\ U_\infty/(f\ c)$. Using this length, the low-pass filtered structures correspond to a streamwise length of $l_x/c > 0.5$. The location of the peak in the low-frequency (blue) region in Figure 5a indicates that the dominant frequency is $f = 25$ Hz, corresponding to a spatial length of $l_x/c = 1$, suggesting that these structures span a full chord length which is consistent with the structures in Figure 10. In contrast to the structures observed in Figure 9, the low-frequency peak in the surface-pressure energy spectrum does not appear to be caused by coherent vortical structures. In fact, the vorticity fields in Figure 10c and f indicate a shear layer originating at the leading edge of the airfoil. It may be assumed that a moving (flapping) shear layer of the separating flow is responsible for the observed low-frequency peak in the surface-pressure energy spectrum. The flapping frequency can be described as a Strouhal number, based on the obstructed area of the flow, $St = f\ c\ \sin(\alpha)/U_\infty$. The frequency-peak at $f = 25$ Hz corresponds to $St = 0.04$, which is comparable to a frequency of $St = 0.03$ found by Zaman et al. (1989).

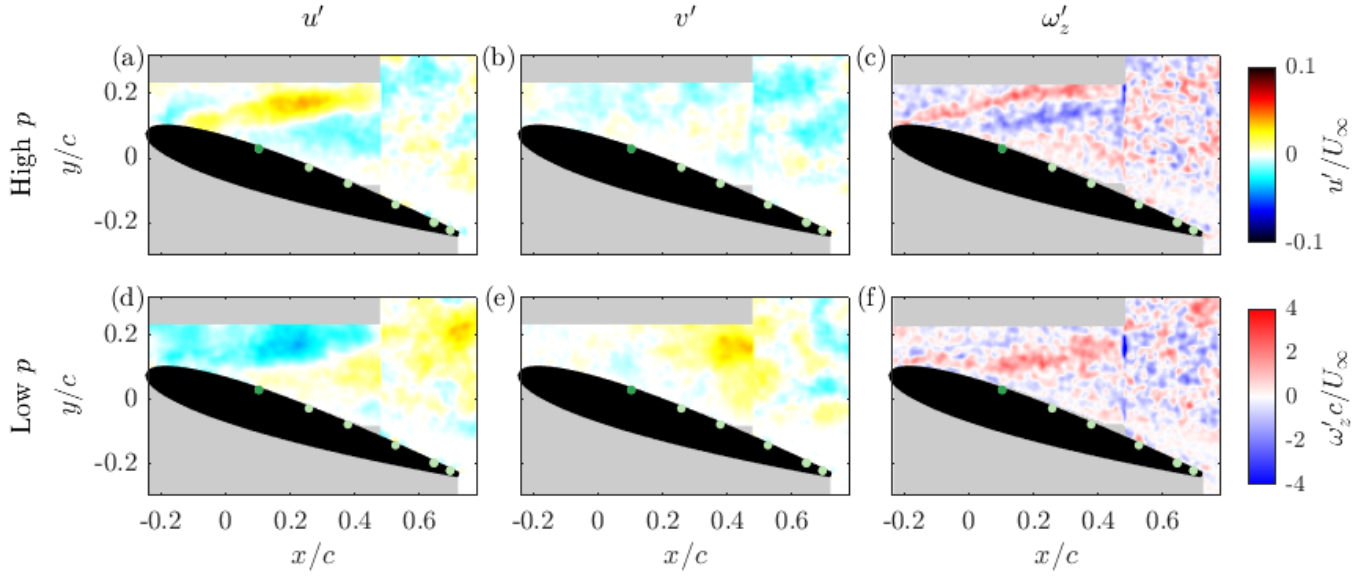

Fig. 10 Velocity and vorticity fields conditioned to high- (a, b and c) and low- (d, e and f) surface pressure events. Surface pressure is low-pass filtered at $f = 50$ Hz.

The velocity fields associated with low- and high-surface-pressure events of the band-pass filtered ($f = 50$–200 Hz) pressure signal are presented in Figure 11. Comparison of these flow structures to

the structures observed in Figure 9 shows great similarity, indicating that they are the dominant structures causing surface-pressure events. The dominance of this frequency band is also apparent in Figure 5a where this frequency band has the highest peak and in Fig. 5b where the band-pass filtered (red line) and unfiltered (black line) signals largely follow the same trend. Using Taylor's hypothesis, the structures in this frequency band (f = 50–200Hz) can be expected to have a streamwise length of approximately l_x/c = 0.125–0.5 with the peak (f = 100 Hz) around l_x/c = 0.25. Indeed, the streamwise length of the observed flow structures in Figure 11 is approximately 0.25c. As discussed above these structures correspond to a train of alternating vortices in the separated shear layer. As these vortices are advected downstream the regions of positive and negative velocity perturbations alternate temporally, causing a varying pressure at the surface of the airfoil.

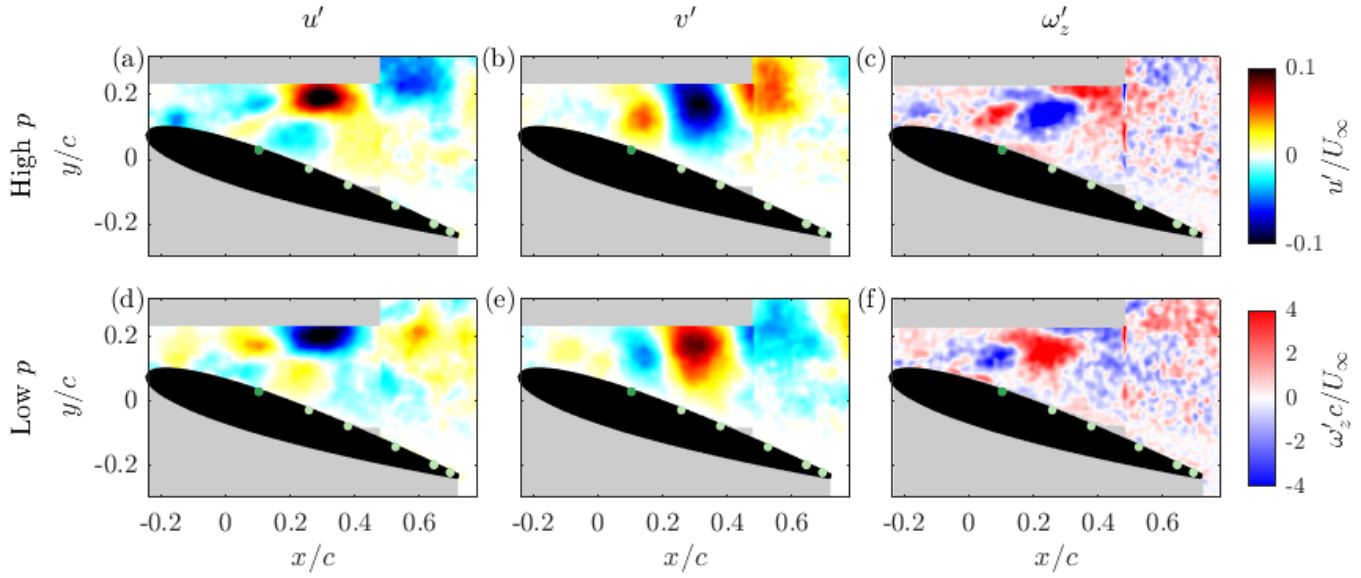

Fig. 11 Velocity and vorticity fields conditioned to high- (a, b and c) and low- (d, e and f) surface pressure events. Surface pressure is band-pass filtered between f = 50-200 Hz.

The velocity fields conditioned to low- and high-surface-pressure events for the high-pass filtered (f > 200 Hz) pressure signal are presented in Figure 12. Structures in this frequency band are expected to have a streamwise length of l_x/c < 0.125. As can be observed in Figure 5a (green band) most of the energy in this frequency band is near the cut-off frequency. Indeed, the observed length of the structures is approximately $l_x/c \approx 0.125$, corresponding to the cut-off frequency of 200 Hz. Similar to the structures in the band-pass filtered frequency band discussed above, these structures correspond to a train of alternating vortices in the shear layer of the separated flow as is visible in Figures 12c and f.

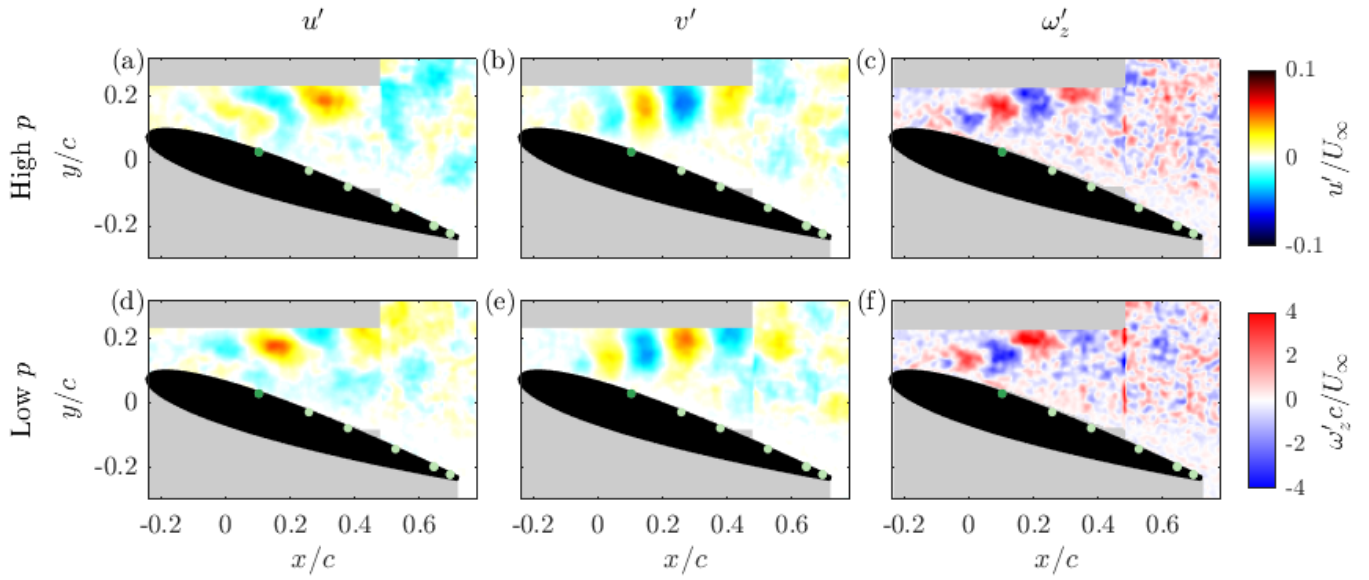

Fig. 12 Velocity and vorticity fields conditioned to high- (a, b and c) and low- (d, e and f) surface pressure events. Surface pressure is high-pass filtered at $f = 200$ Hz.

The above analysis shows that different flow structures are responsible for different peaks in the energy spectrum of the surface-pressure signal. By conditionally averaging the flow based on distinct frequency bands of the surface-pressure signal, the coherent flow structures corresponding to these frequency bands are identified.

3.6. Dynamics of the flow during high-pressure events (POD mapping)

The conditionally-averaged flow fields as presented in Figure 9 can be mapped onto the POD modes as discussed in Section 3.2 and presented in Figure 4. This mapping indicates which dynamic modes of the total flow are important for these conditional averages. Whereas 200 modes are required to represent 50% of the energy of the full velocity field, only 20 modes are required to represent 50% of the energy of these conditional averages. This suggests that the conditional averages are much more dominated by coherent structures, which was also apparent in the above results and clearly visible in Figure 9. The four most dominant dynamic modes in this conditional average are modes 2, 6, 5 and 4 from the full flow field (all presented in Figure 4). While these four modes combined contain less than 4% of the energy of the total flow, they contain 23% of the energy of the conditional average presented in Figure 9. In fact, the global shape of the conditionally averaged velocity fields can be reconstructed using only these four modes as presented in Figure 13c and d (compare to reconstruction using 20 modes containing 50% of kinetic energy in e and f).

The difference in relative energy content of the most energetic modes for the full flow compared to the conditional averages indicates that while many dynamic modes are present in the flow, the conditional averages are dominated by only a handful of dynamic modes. This comparison also suggests that the coherent structures in the conditional averages only make up a small portion of the energy in the full flow field. This means that the largest pressure fluctuations on the surface of the airfoil are a result of only a small part of the energy in the flow.

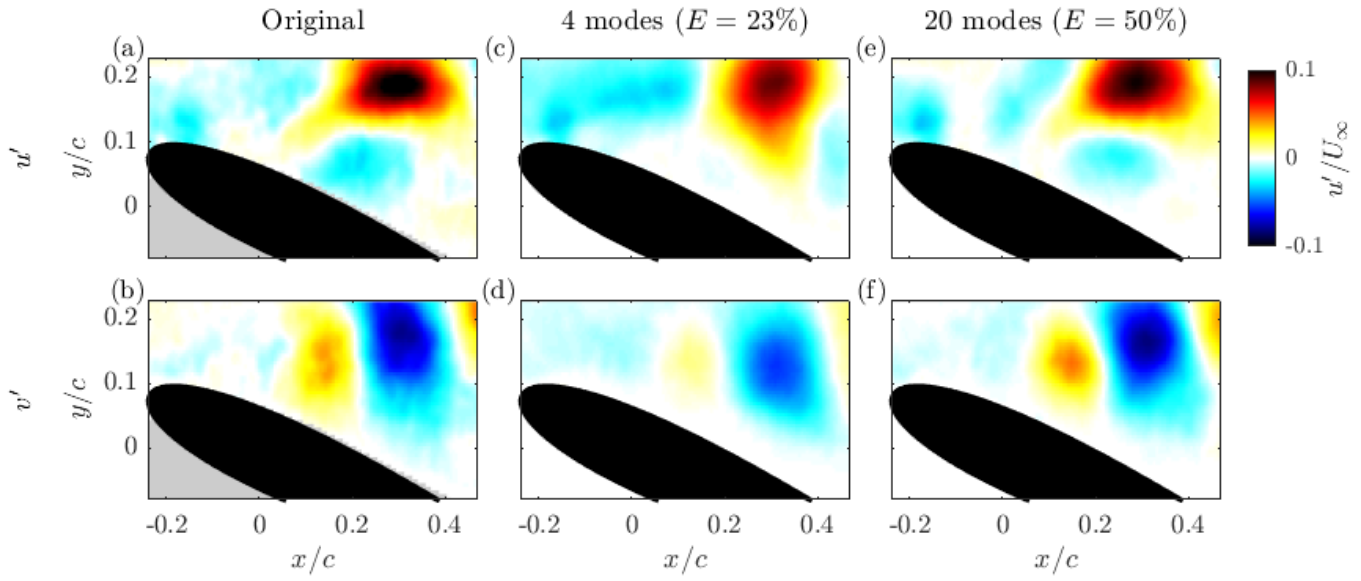

Fig. 13 Conditionally averaged velocity fields (a, b) reconstructed using the 4 (c, d) and 20 (e, f) most energetic POD mode shapes.

4. Conclusions

The present study has analysed the separated flow over a stalled airfoil and the effect of structures in the flow on the surface pressure at the airfoil. Results from POD analysis of the flow, cross-correlation between the surface pressure and the flow and conditionally averaging of the flow conditioned to high-pressure events all indicate coherent structures in the flow responsible for pressure events at the surface. While POD and cross-correlation are both mathematical operators applied to a full time-series, conditional averaging indicates which structures can be expected in the flow during a high-pressure event at the surface. This enables real-time control of such structures by using only the pressure signal at the surface (see for example Abbassi et al. (2017) in which structures in the flow are controlled in real-time based on a skin-friction signal at the surface).

References

Abbassi MR, Baars WJ, Hutchins N, Marusic I (2017) Skin-friction drag reduction in a high-Reynolds-number turbulent boundary layer via real-time control of large-scale structures, *Int. J. Heat Fluid Flow*, 67:30-41.

Amitay M, Glezer A (2002) Role of actuation frequency in controlled flow reattachment over a stalled airfoil. *AIAA J.*, 40:209-216.

Brooks T, Marcolini M, Pope D (1984) Airfoil trailing edge flow measurements and comparison with theory, incorporating open wind tunnel corrections. *9th Aeroacoustic conference*, 2266.

Burgmann S, Brücker C, Schröder W (2006) Scanning PIV measurements of a laminar separation bubble. *Exp. Fluids*, 41:319-326.

Dunne R, McKeon BJ (2015) Dynamic stall on a pitching and surging airfoil. *Exp. Fluids*, 56:157.

Iaccarino G, Ooi A, Durbin PA, Behnia M (2003) Reynolds averaged simulation of unsteady separated flow. *Int. J. Heat Fluid Flow*, 24:147-156.

Kiya M, Sasaki K (1985) Structure of large-scale vortices and unsteady reverse flow in the reattaching zone of a turbulent separation bubble. *J. Fluid Mech.*, 154:463-491.

Mariappan S, Gardner AD, Richter K, Raffel M (2014) Analysis of dynamic stall using dynamic mode decomposition technique. *AIAA J.*, 52:2427-2439.

Sirovich L (1987) Turbulence and the dynamics of coherent structures. Part I: Coherent structures. *Q Appl Math*, XLV:561-571.

Thomareis N, Papadakis F (2017) Effect of trailing edge shape on the separated flow characteristics around an airfoil at low Reynolds number: a numerical study. *Phys. Fluids*, 29:014101.

Zaman KBMQ, McKinzie DJ, Rumsey CL (1989) A natural low-frequency oscillation of the flow over an airfoil near stalling conditions. *J. Fluid Mech.*, 202:403-442.